

# Design of a Satellite Solar Panel Deployment Mechanism Using the Brushed DC Motor as Rotational Speed Damper

Hossein Ramezani Ali-Akbari

**Abstract**—This paper presents an innovative method to control the rotational speed of a satellite solar panel during its deployment phase. A brushed DC motor has been utilized in the passive spring driven deployment mechanism to reduce the deployment speed. In order to use the DC motor as a damper, its connector terminals have been connected with an external resistance in a closed circuit. It means that, in this approach, there is no external power supply in the circuit. The working principle of this method is based on the back electromotive force (or back EMF) of the DC motor when an external torque (here the torque produced by the torsional springs) is coupled to the DC motor's shaft. In fact, the DC motor converts to an electric generator and the current flows into the circuit and then produces the back EMF. Based on Lenz's law, the generated current produced a torque which acts opposite to the applied external torque, and as a result, the deployment speed of the solar panel decreases. The main advantage of this method is to set an intended damping coefficient to the system via changing the external resistance. To produce the sufficient current, a gearbox has been assembled to the DC motor which magnifies the number of turns experienced by the DC motor. The coupled electro-mechanical equations of the system have been derived and solved, then, the obtained results have been presented. A full-scale prototype of the deployment mechanism has been built and tested. The potential application of brushed DC motors as a rotational speed damper has been successfully demonstrated.

**Keywords**—Back electromotive force, brushed DC motor, rotational speed damper, satellite solar panel deployment mechanism.

## I. INTRODUCTION

SPACE flight achievements affect both the theoretical science and the practical applications in the realm of space structures and mechanisms. Spacecraft structures such as large solar panels, antennas and gravity gradient booms due to their size often need to be compacted for ground transportation and launched and deployed at the time of on-orbit operation. The deployment of these structures can be performed by the large elastic deformations or the deployment mechanisms. In case of deployment mechanisms, the movement of these mechanisms is used to expand the spacecraft structures. Due to the difficult and impractical mechanical repairing of such mechanisms in space, they must be more reliable than ordinary mechanisms on the earth. The high launch vibrations, micro-gravity environment and power restrictions are also important parameters which must be considered in the mechanical design [1]. A space mechanism commonly consists of the

mechanical parts such as gears, springs, linkages, dampers, latches, cams which are assembled and worked together to achieve its operational goal.

To be particular, we focus on the satellite solar panel deployment mechanisms. The deployable solar panels are stowed during the launch into a permitted small size volume in the launcher fairing and then expanded on-orbit, so the satellite has opportunity to provide very larger area for installing the solar cells exposure to the sun light rather than body-mounted solar panels. When the deployment phase of an expandable solar panel finishes then it becomes fixed at an intended position by locking at the hinges to start its mission as the power supply of the satellite. This locking operation can cause undesirable oscillatory or impulsive forces and moments on the satellite. Therefore, to reduce the effects of these mechanical fluctuations, a device which controls the deployment speed of the solar panel up to an accepted level is needed. Several types of deployment speed damper have been used to control the deployment rate of satellite solar panels such as liquid-based viscous dampers [2]-[4], paraffin actuators [5], mechanical brakes [6], [7], and eddy current dampers (ECDs) [8], [9] which are recently utilized in great deal of aerospace applications as rotational speed damper. Each of these devices has some disadvantages, for instance, the damping coefficient of liquid-based viscous dampers is sensitive with respect to the environmental temperature, and the low pressure vacuum condition in the space may result in outgas of the viscous liquid inside the damper [2]. Furthermore, the rotary viscous dampers need a precise fabrication process to avoid producing air bubbles in the liquid inside the damper [3]. The paraffin actuators need electrical power to melt the paraffin inside the actuator to release the mechanism to move and also melting the paraffin is a time-consuming process. The mechanical brakes are simpler to fabricate, but due to existence of mechanical friction between preloaded parts, their reliability is lower than other approaches and some unwanted mechanical vibrations may appear. Most of these imperfections have been removed in ECDs. They have some unique properties such as non-contact, non-leakage and simple fabrication which make them a good candidate for aerospace applications [8]. The working principle of ECDs relies on the interaction between a non-magnetic conductive material and a time varying magnetic field. The variation of the magnetic field due to the movement of magnet or the non-magnetic conductive part causes generating the eddy currents in the non-magnetic conductive part. The generated eddy

Hossein Ramezani Ali-Akbari is with the Iranian Space Research Center, Satellite Research Institute, Saadat-Abad Ave., Tehran, Iran (e-mail: hrhaliakbari@yahoo.com).

currents induce a magnetic field with opposite polarity with respect to the applied magnetic field and a repulsive EMF, as well. The generated eddy currents are dissipated into the heat because of the internal resistance of the non-magnetic conductive part and the kinetic energy of the moving system decreases [10], [11].

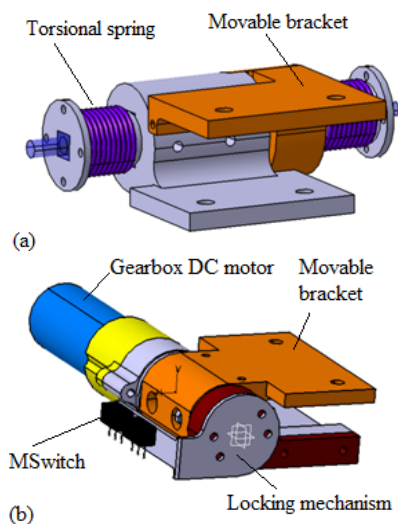


Fig. 1 Photograph of the 3D CAD model of (a) the active hinge and (b) the passive hinge

In this paper, the potential application of brushed DC motors as damper for controlling the rotational speed of the solar panel during its deployment phase has been studied, and a prototype of mechanism has been manufactured and tested. The test results have demonstrated a good functional performance. The solar panel deployment mechanism includes two parts (see Fig. 1); (1) an active hinge which provides the kinetic energy of deployment by two redundant torsional springs, (2) a passive hinge which controls the rotational speed by means of a brushed DC motor and undergoes locking in the intended position when the solar panel deployment phase finishes. Two redundant micro-switches have been mounted on the passive hinge to notify that the solar panel deployment phase has been completed and the locking successfully has been performed. In order to use the DC motor as a damper, its connector terminals are connected to a variable external resistance without any external power supply. It means that there is no external electrical power supply in the closed circuit and the kinetic energy of the system is provided by a part of stored potential energy into the torsional springs converted to the kinetic energy of the moving solar panel and the rest dissipates by the brushed DC motor and leads to reducing the deployment speed. Similar to ECDs, in this approach, there is no physical contact to produce friction and no risk of leakage.

The working principle of this method is based on the back EMF produced by the DC motor. The coupled external torque causes rotating the motor's shaft similar to an electric generator and the electric current flows into the circuit and induces the back EMF. Based on Lenz's law, the generated

current produced a torque which acts in opposite of applied external torque, i.e. the torque exerted by torsional springs, thus, it causes to reduce the rotational speed of the solar panel. Due to the short angular distance where the solar panel travels from  $0^\circ$  (the stowed position) to  $90^\circ$  (the full deployed position) during its deployment phase (see Fig. 2), a small amount of back EMF is induced into the DC motor and it cannot sufficiently affect the high external torque of the torsional springs. To solve this problem, a gearbox has been assembled to the DC motor which magnifies the number of turns which the DC motor experiences. As a result, a sufficient amount of current flows into the DC motor closed circuit which strengthens the back EMF effect. Unlike the ECDs, we can easily set an intended damping coefficient to the system by means of the variable external resistance. By changing the external resistance, the amount of current which flows in the circuit can be controlled.

## II. THE BACK EMF

When the electric current flows into the rotor conductors of the DC motor which are located in a magnetic field, a torque is exerted on the rotor shaft. However, due to the rotation of the coil, the conductors themselves cut the magnetic flux that it results in generating a back EMF whose magnitude can be calculated by means of the Faraday's law of induction [12]. This law states that the induced back EMF ( $e$ ) is computed by the rate of change of the magnetic flux ( $\Phi_e$ ) as:

$$e = -\frac{d\Phi_e}{dt} \quad (1)$$

The back EMF can be expressed using the angular speed of the motor as [13]:

$$e = k_e \omega \quad (2)$$

where  $k_e$  is the back EMF constant, and  $\omega$  is the angular speed of the motor.

## III. THE BASIC EQUATIONS OF THE DC MOTOR

The dynamic behavior of DC motors can be described by two equations; the first equation describes the electrical behavior, and the second one describes the mechanical behavior. These equations are presented in the following sections in detail. It has to be noted that the explanations and mathematical equations which are presented in this section have been rewritten from [12].

### A. The Electrical Equation

The rotor of the DC motor is assumed to be a single coil characterized by inductance  $L$  and resistance  $R$ . By taking into account the back EMF of the motor, the electrical equation of the closed circuit can be written as:

$$V = L \frac{di}{dt} + Ri + e \quad (3)$$

where  $V$  is the electric terminal voltage and  $i$  is the electric current flows into the closed circuit.

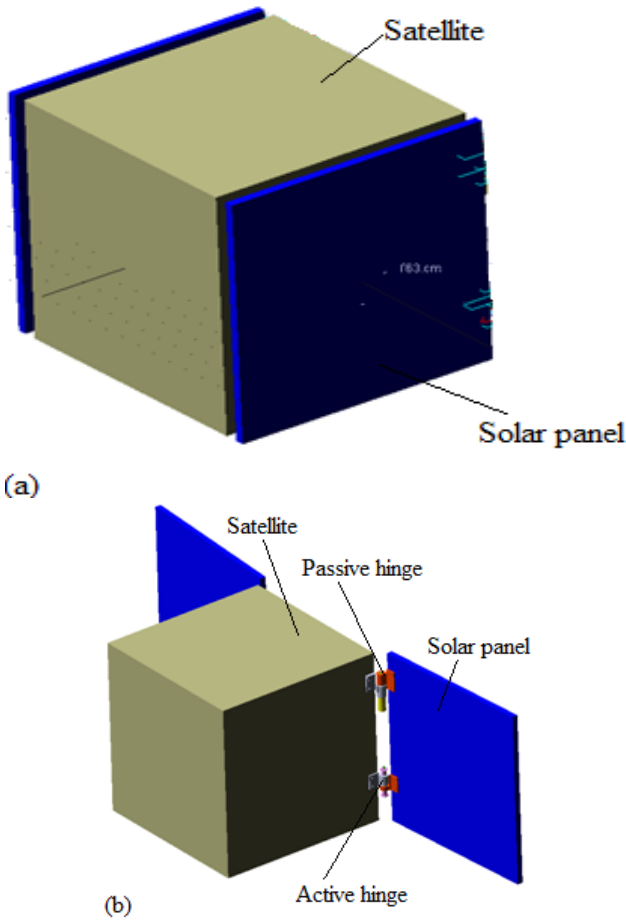


Fig. 2 Schematic view of the satellite when the solar panels are (a) stowed and when the solar panels are (b) full deployed

### B. The Mechanical Equation

When a DC motor supplied by the external voltage, it exerts a torque. This torque acts on the mechanical structure, which is characterized by the rotor inertia  $J$  and the internal viscous friction coefficient  $F$ . Obviously, in any operating environment, there is a load torque which is exerted on the motor. Therefore, the following equation can be written as:

$$T_M - T_L = J\dot{\omega} + F\omega \quad (4)$$

where  $T_L$  is the load torque.

### C. Geared DC Motors

In this case, a gearbox is introduced between the motor and the load, thus it causes reducing the output angular velocity of the motor. To correctly understand the effects of the gearbox, the first thing to state is that damping and inertia are not the same if measured at the input or output of the gearbox. We denote the internal damping and inertia of the gearbox as  $F_G$  and  $J_G$ , respectively. Then, notice that the torque and angular

velocity exerted by the motor are the same at the input of the gearbox and at the output. They are denoted by  $T'_M$  and  $\omega'$ , respectively. Therefore, the relation between the power at the input and output of the gearbox can be written as:

$$T_M \omega = T'_M \omega' \quad (5)$$

and, since  $\omega' = \omega/n$  and  $T'_M = nT_M$ .

Substituting the above equations in (4), and taking into account the increase of the damping and inertia due to the gearbox, it turns out:

$$T'_M - T_L = (J_G + n^2 J) \dot{\omega}' + (F_G + n^2 F) \omega' \quad (6)$$

By a comparison between (4) and (6), it is found that the presence of the gearbox highly increases the inertia and the damping of the motor from the point of view of the load.

### IV. THE EQUATION OF MOTION OF THE SOLAR PANEL

Consider the solar panel and the deployment mechanism with together as a single degree of freedom torsional system with a viscous damper. The equation of motion can be derived as:

$$J_s \ddot{\theta} + F_H \dot{\theta} + k_s \theta = 0 \quad (7)$$

where  $J_s$  is the mass moment of inertia of the solar panel with respect to the hinge axis,  $F_H$  is the viscous friction damping coefficient of the hinge,  $k_s$  is the torsional spring constant of the system.  $\theta$  is the angular displacement of the solar panel.

### V. THE COUPLED ELECTRO-MECHANICAL SYSTEM OF EQUATIONS

In this section, a coupled electro-mechanical system of differential equations which describes the dynamic behavior of the solar panel-DC motor system is derived. To this end, the electric and mechanical equations of the DC motor have been combined with the equation of motion of the solar panel and some manipulations should be performed. Due to utilizing the DC motor as deployment speed damper, the electric power supply is removed from the closed circuit, thus in (3) the voltage is set to zero, i.e.  $V = 0.0$ , and just the induced voltage by the back EMF remains (see Fig. 3). In this case, the DC motor acts like an electric power generator and the generated electric current flows into the closed circuit. To control the amount of the generated current, a variable external resistance  $R_{ext}$  is put in the circuit between the two connector terminals of the DC motor. There is a gearbox between the torque load (exerted by the torsional springs) and the DC motor. Therefore, the gearbox magnifies the rotational speed which the DC motor experiences, i.e.  $\omega = n\dot{\theta}$ , and as a result more electric current or, in the other words, more EMF is generated. The EMF like an external power supply causes

producing an output torque from the motor which based on Lenz's law acts in opposite of the applied external torque load. Due to presence of the gearbox the exerted torque of the DC motor is multiplied by factor  $n$  in the output of the gearbox. Considering the above explanations and combining the electrical and mechanical equations of the DC motor and the solar panel, one can obtain:

$$L \frac{di_e}{dt} + R_{tot} i_e + k_e n \dot{\theta} = 0 \quad (8a)$$

$$J_{tot} \ddot{\theta} + F_{tot} \dot{\theta} + k_s \theta - k_t n i_e = 0 \quad (8b)$$

where  $i_e$  is the electric current generated because of the EMF. The terms  $R_{tot}$ ,  $J_{tot}$ , and  $F_{tot}$  are the total resistance in the closed circuit, the total mass moment of inertia, and the total viscous friction damping coefficient of the system, respectively, and they can be formulated as:

$$R_{tot} = R + R_{ext} \quad (9)$$

$$J_{tot} = J_s + J_G + n^2 J \quad (10)$$

$$F_{tot} = F_H + F_G + n^2 F \quad (11)$$

The term  $k_t n i_e$  in (8b) is the generated torque of the motor due to the EMF which is multiplied by factor  $n$  at the output of the gearbox.

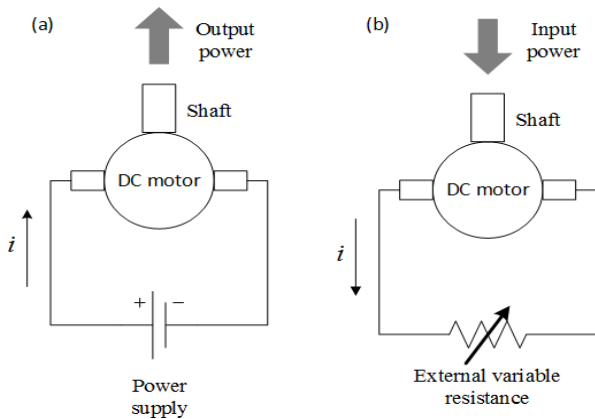


Fig. 3 Schematic views of a brushed DC motor in the closed circuit applied as (a) a driver and as (b) a rotational speed damper

## VI. NUMERICAL RESULTS

### A. The Electrical and Mechanical Properties of the Geared DC Motor

A geared brushed DC motor model 2232U012SR is selected as rotational speed damper which is made by FAULHABER drive systems company (see Fig. 4). Based on the motor's datasheet [14], the electrical and mechanical characteristics of the motor are presented in Table I. The mechanical properties of the gearbox (series 22/7) also are provided in [15] and represented in Table I. As it can be seen from Table I, the

values of gearbox rotational inertia and its viscous friction damping coefficient have been not filled because these data have been not reported in the motor's datasheet. These values are very smaller than the solar panel inertia and the viscous damping friction of the hinges, i.e.  $J_G \ll J_s$  and  $F_G \ll F_H$ , thus, we set them to zero in the dynamic simulation of the system.

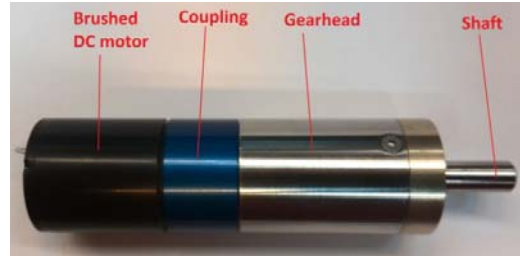


Fig. 4 Photograph of the geared brushed DC motor model 2232U012SR

TABLE I  
 THE ELECTRICAL AND MECHANICAL PROPERTIES OF THE GEARED DC MOTOR

Symbol	Definition	Value
$R$	Terminal resistance	$4.09 \Omega$
$k_e$	Back-EMF constant	$100.8 \times 10^{-3} \text{ Vs}$
$k_t$	Torque constant	$16 \times 10^{-3} \text{ Nm/A}$
$L$	Rotor inductance	$18 \times 10^{-5} \text{ H}$
$J$	Rotor inertia	$3.8 \times 10^{-7} \text{ kgm}^2$
$F$	Motor viscous friction damping coefficient	$3.77 \times 10^{-7} \text{ Nm.rad/s}$
$\eta_{max}$	Maximum efficiency	%86
$n$	Gearbox reduction ratio	159:1
$\eta_G$	Gearbox efficiency	%60
$J_G$	Gearbox inertia	-
$F_G$	Gearbox viscous friction damping coefficient	-

### B. Solving the Coupled Electro-Mechanical System of Equations

In this section, the coupled electro-mechanical system of differential equations (8) is numerically solved. The mass ( $m$ ) and rotational inertia ( $J_s$ ) of the honeycomb solar panel are  $2 \text{ kg}$  and  $0.18 \text{ kg.m}^2$ , respectively. The dimensions of the solar panel are  $60 \times 60 \times 2 \text{ cm}$ . The viscous friction damping coefficient of the hinges considered as  $F_H = 0.001 \text{ Nm.rad/s}$  which is the viscous damping coefficient of the hinge ball bearings. The spring constant which is a summation of two torsional springs is  $k_s = 0.15 \text{ Nm/rad}$ . It has to be noted that, the torsional springs have been preloaded by twisting them up to  $180^\circ$ , and as a result in the full deployed position just the solar panel rotates up to  $90^\circ$ . It means that still there is a spring-preload on the hinge which it can be useful for the locking of the solar panel at the end of the deployment phase.

Then, using the obtained parameters and the coupled electro-mechanical equation of the system (8) and considering the different values of the external resistance in the closed circuit, the dynamic behavior of the solar panel during its

deployment phase has been simulated. The system of differential equations (8) is solved by MATLAB's ode45 solver and the obtained results for the solar panel rotational displacement and speed are plotted in Figs. 3 and 4, respectively. From Fig. 3, it can be seen that the increment in the external resistance leads to decreasing the deployment time duration of the solar panel. As it can be found from the Fig. 3 if the external resistance is removed from the closed circuit, i.e.  $R_{ext} = 0.0$ , the deployment time reaches to its maximum. Therefore, by trial and error, a suitable value for the external resistance can be obtained based on the intended deployment time. From the obtained results, when the external resistance is set to 50 Ohm, the solar panel reaches to its full deployed position in 6.8 s and for the lower values of the external resistance such as 30, 20, and 10 Ohm, the deployment phase takes the time more than 10 s. From Fig. 4, it can be found that the rotational speed of the solar panel increases while the external resistance increases and also it increases the nonlinear reduction of the rotational speed over the time from 0 to 10 s. The results show that if the external resistance is removed from the closed circuit, the angular velocity of the solar panel reduces to 1.35 deg/s and it remains nearly unchanged when time pasts and the angular acceleration approximately reaches to zero. But inversely, when a high value resistance is put into the closed circuit, for instance 50 Ohm, the angular velocity of the solar panel reaches to 17.2 deg/s and then nonlinearly decreases over time and the solar panel experiences an accelerated rotational motion during its deployment phase. Thus, the deployment duration time, the solar panel rotational acceleration in the release stage and during the deployment phase, the rotational speed at the locking position at the end of the deployment phase are parameters which must be considered to select an optimum value for the external resistance. As earlier mentioned, the full-scale prototype of the solar panel deployment mechanism has been manufactured and its functional performance has been tested. It should be noted that an equivalent aluminum-made frame has been used instead of the honeycomb solar panel which has the same mass and rotational inertia (see Fig. 7). The experimental results show that when the external variable resistance is set to 50 Ohm, it takes approximately 10 seconds to deploy the solar panel from  $0^\circ$  to  $90^\circ$ . Due to the manufacturing tolerances, misalignments and imperfections in the part assembling, there is a little difference between the theoretical simulations and experimental results. But, the experimental results still are in good agreement with those obtained from theoretical simulation, and the concept of using the geared brushed DC motors as a rotational speed damper is successfully approved.

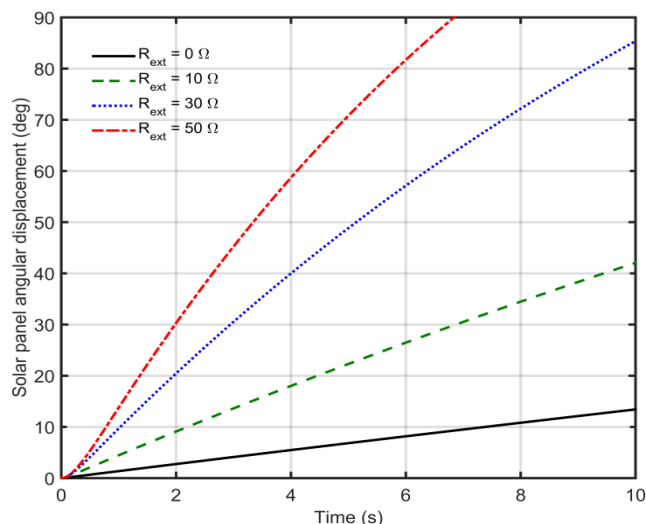


Fig. 5 Effect of the external variable resistance on the deployment duration time

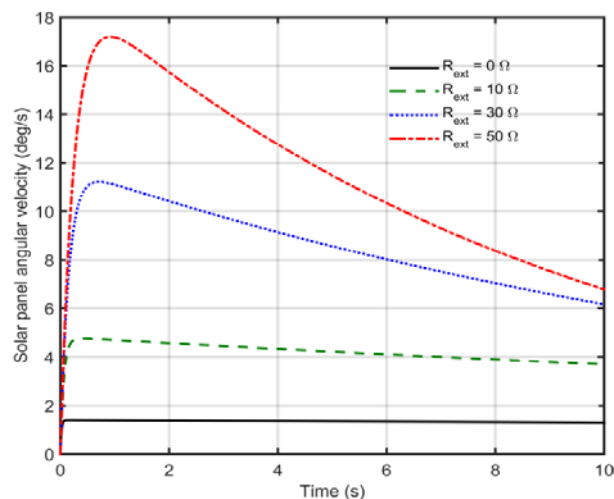


Fig. 6 Effect of the external variable resistance on the solar panel angular velocity

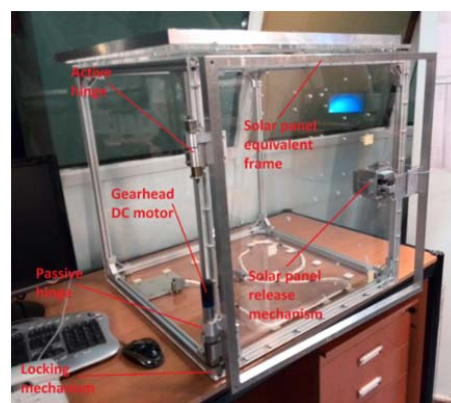


Fig. 7 Functional test stand of the solar panel deployment mechanism using a solar panel equivalent frame

## VII. CONCLUSION

The potential application of brushed DC motors as

rotational speed damper for satellite solar panel deployment mechanism is demonstrated. The coupled electro-mechanical system of differential equations for the solar panel-deployment mechanism is derived. Then, this system of differential equations is numerically solved for a real practical case. The obtained results reveal that the brushed DC motor can act as a rotational speed damper and by changing the external variable resistance in the closed circuit, it can be possible to set an intended speed damping coefficient to the system. Furthermore, it can be found that the rotational velocity of solar panel increases while the external resistance increases. Based on this concept, a real full-scale prototype has been built and tested. The test results are in good agreement with the ideal theoretical simulations. The presented concept and results in this article can be used in design, analysis and manufacturing of rotational deployment mechanisms.

#### REFERENCES

- [1] A. W. Bergquist, J. M. Jensen, B. J. Santiestevan, A. T. Vaughan, C. P. Vlastelica, C. D. Weaver, "Structures, mechanisms, launch vehicle selection," Academic Course Report, Aerospace and Ocean Engineering Department, Virginia Tech, Blacksburg, VA. 2001.
- [2] W. Shapiro, F. Murray, R. Howarth, and R. Fusaro, "Space mechanisms lessons learned study," *NASA TM-107046 and TM-107047*, vols. I and II, 1995.
- [3] M. C. Calassa, and R. Kackley, "Solar array deployment mechanism," The 29<sup>th</sup> Aerospace Mechanisms Symposium, pp. 79-92. 1995.
- [4] R. Stengel, "Spacecraft Mechanisms," Lectures on Space System Design-Princeton University, MAE 342. 2008.
- [5] G. Sneiderman, "Performance measurement of the sub-millimeter wave astronomy satellite (SWAS) solar array deployment system," NASA, Goddard space flight center, Special payloads division, Greenbelt, Maryland 20771, 1995, Technical note.
- [6] M. G. El-Sherbiny, A. Khattab, and M. K. Kassab, "Design of the deployment mechanism of solar array on a small satellite," *American Journal of Mechanical Engineering*, vol. 1, No. 3, pp. 66-72. 2013.
- [7] G. F. Abdelal, A. Bakr Elhady, and M. Kassab, "Design of a deployment rotation mechanism for micro-satellite," *International Journal for Simulation and Multidisciplinary Design Optimization*, vol. 3, pp. 289-296. 2009.
- [8] Q. Pan, T. He, D. Xiao, and X. Liu, "Design and damping analysis of a new eddy current damper for aerospace applications," *Latin American Journal of Solids and Structures*, vpl. 13, No. 11, pp. 1997-2011. 2016.
- [9] "Durango eddy current damper product catalog and design guidelines," Avior Control Technologies, Inc., 2017. ([www.AviorControls.com](http://www.AviorControls.com))
- [10] H. A. Sodano, and J.-S. Bae, "Eddy current damping in structures," *Shock and Vibration Digest*, vol. 36, No. 6, pp. 469-478. 2004.
- [11] J.-S. Bae, M. K. Hwak, and D. J. Inman, "Vibration suppression of a cantilever beam using eddy current damper," *Journal of Sound and Vibration*, vol. 284, Issues 3-5, pp. 805-824. 2005.
- [12] L. Zaccarian, "DC motors: dynamic model and control techniques," Teaching Material, [homepages.laas.fr/lzaccari/seminars/DCmotors.pdf](http://homepages.laas.fr/lzaccari/seminars/DCmotors.pdf), Accessed on 18<sup>th</sup> November 2017.
- [13] I. Vollmecke, "Parameter identification of DC motors," Technical Report, [www.imc-berlin.com](http://www.imc-berlin.com), Accessed on 18<sup>th</sup> November 2017.
- [14] F. Faulhaber, "DC-micromotors, Series 2232U," Product Datasheet, [www.faulhaber.com](http://www.faulhaber.com), Accessed on 18<sup>th</sup> November 2017.
- [15] F. Faulhaber, "Planetary Gearheads, Series 22/7," Product Datasheet, [www.faulhaber.com](http://www.faulhaber.com), Accessed on 18<sup>th</sup> November 2017.

**Hossein Ramezani Ali-Akbari** was born on October 21, 1984. He received his B.Sc. in Aerospace Engineering from Malek Ashtar University of Technology, Isfahan, Iran, in 2008. He then received his M.Sc. in Aerospace Engineering from Sharif University of Technology, Tehran, Iran, in 2011. He works as an aerospace engineer at Iranian Space Research Center, Satellite Research Institute (SRI), since 2011, and his current focus is on the spacecraft mechanism design.